Two-Phase Computerized Planning of Cryosurgery Using Bubble-Packing and Force-Field Analogy

Daigo Tanaka
Department of Biomedical Engineering,
Carnegie Mellon University,
5000 Forbes Ave.,
Pittsburgh, PA 15213

Kenji Shimada
Department of Mechanical Engineering
and Department of Biomedical Engineering,
Carnegie Mellon University,
5000 Forbes Ave.,
Pittsburgh, PA 15213

Yoed Rabin[1]
Department of Mechanical Engineering,
Carnegie Mellon University,
5000 Forbes Ave.,
Pittsburgh, PA 15213
e-mail: rabin@cmu.edu

***Background**: Cryosurgery is the destruction of undesired tissues by freezing, as in prostate cryosurgery, for example. Minimally invasive cryosurgery is currently performed by means of an array of cryoprobes, each in the shape of a long hypodermic needle. The optimal arrangement of the cryoprobes, which is known to have a dramatic effect on the quality of the cryoprocedure, remains an art held by the cryosurgeon, based on the cryosurgeon's experience and "rules of thumb." An automated computerized technique for cryosurgery planning is the subject matter of the current paper, in an effort to improve the quality of cryosurgery.* ***Method of Approach**: A two-phase optimization method is proposed for this purpose, based on two previous and independent developments by this research team. Phase I is based on a bubble-packing method, previously used as an efficient method for finite element meshing. Phase II is based on a force-field analogy method, which has proven to be robust at the expense of a typically long runtime.* ***Results**: As a proof-of-concept, results are demonstrated on a two-dimensional case of a prostate cross section. The major contribution of this study is to affirm that in many instances cryosurgery planning can be performed without extremely expensive simulations of bioheat transfer, achieved in Phase I.* ***Conclusions**: This new method of planning has proven to reduce planning runtime from hours to minutes, making automated planning practical in a clinical time frame.* [DOI: 10.1115/1.2136166]

Keywords: cryosurgery, prostate, bubble-packing, force-field analogy, computerized planning

1 Introduction

Cryosurgery is the destruction of undesired biological tissues by freezing. Cryosurgery has been used to treat cancerous tissues in a large variety of clinical applications, such as skin, hemorrhoids, brain, bone, kidney, liver, breast, and prostate cancers [1]; it has great potential as an alternative to conventional surgery, with minimal damage to healthy surrounding tissues.

Minimally invasive cryosurgery is typically performed by means of cryoprobes in the shape of long hypodermic needles, with a sharp pointed tip. The cooling effect is created near the tip of the cryoprobe, using either liquid nitrogen boiling, or the Joule-Thomson cooling effect (the cooling effect associated with sudden change in pressure of gas flowing through a nozzle). Regardless of the cooling technique, the cooling fluid is not brought in direct contact with the tissue, but displaced to the surroundings. The cooling effect creates a frozen region around the tip of the cryoprobe, typically in the shape of an elongated ellipsoid, for a single operated cryoprobe.

Prostate cryosurgery was the first minimally invasive cryosurgical procedure to pass from the experimental stage to routine surgical treatment [2]. The minimally invasive approach created a new level of difficulty in cryosurgery planning in which a predefined three-dimensionally shaped tissue must be treated while preserving the surrounding tissues. To overcome this difficulty, five [3] and six (Erbe Elektromedizin GmbH, Germany) minimally invasive cryoprobe arrangements were suggested during the early 1990s, based on liquid nitrogen cooling. With recent technological developments, the diameter of the cryoprobe has decreased dramatically (Endocare, Inc., CA; Galil-Medical, Inc., Israel). In an effort to gain better control over the cryosurgical procedure, the number of cryoprobes has been increased so that more than a dozen cryoprobes can be applied simultaneously. If effectively localized, one of the potential benefits of a large number of miniaturized cryoprobes is superior control over the freezing process. Naturally, the application of a large number of cryoprobes is cause for debate over cost-effectiveness. Furthermore, inserting a large number of cryoprobes into a small target region (i.e., small organ) may cause additional injury to surrounding healthy tissue. The clinical and technological complications of a cryoprocedure with such a large number of cryoprobes may not yet be fully appreciated.

The so-called urethral warmer is an additional thermal element, typically applied in prostate cryosurgery to reduce destruction to the urethra and thereby prevent postcryosurgery complications (the urethra extends nearly to the center of the prostate). Technically, the urethral warmer is a counterflow water heat exchanger, embodied in a standard catheter. From a reservoir at close-to-core body temperature, the water is pumped through the catheter to maintain the urethra temperature at above freezing. The urethral warmer has been demonstrated to minimize postcryosurgery complications associated with damage to the urethra [4].

To date, cryoprobe localization is an art held by the cryosurgeon and based on the surgeon's own experience and accepted practices. Currently, means for determining optimal location, or

[1]Corresponding author.

Contributed by the Bioengineering Division of ASME for publication in the JOURNAL OF BIOMECHANICAL ENGINEERING. Manuscript received May 13, 2005; final manuscript received September 19, 2005. Review conducted by Elaine P. Scott.

optimal thermal history for the cryoprobes, are limited. Cryoprobes are typically operated in a trial-and-error fashion, until the target area is thought to be frozen. Toward the end of the freezing process, cryoprobes are usually turned on and off in order to achieve a desired coverage of the target region. The need in this process is associated with suboptimal cryoprobe placement, whereas optimal placement may lead to simultaneous operation of all cryoprobes, thereby reducing the duration of the operation. Suboptimal cryoprobe localization may lead to one or more of the following deficiencies: areas in the target region may be left untreated, healthy surrounding tissue may experience cryoinjury, an unnecessary number of cryoprobes may be used, the duration of the surgical procedure may become excessive, and postcryosurgery complications may occur—all of which affect the quality and cost of medical treatment. Computerized planning tools, which are the subject of the current paper, would help to alleviate these deficiencies.

The difficulties in planning a minimally invasive cryoprocedure have been widely acknowledged by other researchers, and efforts to develop computerized means to facilitate planning are reported in the literature. In 1992, Keanini and Rubinsky [5] reported on a numerical optimization technique for prostate cryosurgery planning with the goal of optimizing the number of cryoprobes, their diameter, and their active length. Thus, there were three variables to be optimized. The prostate was modeled as a truncated cone with the urethra as a coaxial cylinder. The locations of the cryoprobes were determined by first dividing the prostate into a number of simplified equiangular subregions equal to the number of cryoprobes (modeling the prostate as an axisymmetric object). One cryoprobe was placed at the center of each subsection. The resulting configuration was a set of cryoprobes placed at equal intervals along the circumference of a circle. The quantity minimized was the ratio of the volume of the frozen extraprostatic tissue to the volume of the prostate, evaluated at the time when the entire prostate became frozen.

Keanini and Rubinsky [5] employed the simplex optimization method, which, in general, is known to work well for linear problems [6,7]. Because of the highly nonlinear nature of the problem of cryoprobe placement, the simplex method is expected to become extremely expensive in computational terms, unless the problem is simplified. In addition, Keanini and Rubinsky suggested fewer parameters to be optimized, where more parameters make the simplex method considerably more expensive. The number of parameters to be optimized includes at least three coordinates for each cryoprobe in an arbitrary three-dimensional (3D) target region, for a dozen cryoprobes or more.

Baissalov et al. [8] have also presented a model for cryosurgery planning. In their model, a thermal simulation algorithm was used to generate temperature distribution around cryoprobes, in order to visualize isotherms in the anatomical region of interest and to provide tools to aid in estimating the amount of freezing damage to the target region and surrounding normal tissues. Their optimization work was semi-empirical, not fully automated, where the empirical nature of the technique is based on the experience of the specific operator.

In a later report, Baissalov et al. [9] demonstrated that it is possible to simultaneously optimize multiple cryoprobe placements and their thermal protocol, using a gradient-descent method [9]. This method requires a large number of consecutive heat transfer simulations, making the cost of planning high and the duration of planning impractical as an intermediate stage of a clinical application. Three different forms of objective function were examined in [9], and it was found that the optimization results were dependent on the initial values of the variables, the form of the objective function, optimization goals, and the mathematical method adopted for gradient calculation.

A prototype of a computerized cryoprobe localization tool has been presented recently by Lung et al. [10]. This tool operates iteratively and relies on a series of bioheat transfer simulations of the cryosurgical procedure. At the end of each simulation, defective regions are identified in which defects are defined as tissue outside the target area that was cryoinjured—or tissue inside the target area that was not cryoinjured. Using a force-field analogy, defective regions apply forces to the cryoprobes, moving them to better locations prior to the start of the next bioheat transfer simulation. This process of simulation and cryoprobe displacement repeats until no additional improvement is achieved.

This force-field analogy technique has been proven numerically efficient in two dimensions, on representative cross sections of the prostate [10]. This technique eliminates the need for gradient calculations and allows repositioning of a number of cryoprobes after each heat transfer simulation. The force-field analogy has been demonstrated to be efficient, robust, and insensitive to initial conditions, even in more complex cases where additional heating elements are applied to assist in shaping the frozen region [11]. These heating elements are termed "cryoheaters," but are not yet available for clinical applications [12].

Our long-term goal is to develop a computerized planning tool for cryosurgery that takes a 3D reconstruction of a target region from an available imaging device (such as ultrasound or MRI) and suggests the best cryoprobe localization. To be useful, the tool must be able to perform full-scale 3D planning in a few minutes, while the patient is on the operating table. The current report presents a new technique for computerized planning of cryosurgery based on the bubble-packing method [13–15]. The new technique is orders of magnitude faster than the previous techniques reviewed above. The bubble-packing technique is compared to the previously most efficient technique, which is based on force-field analogy. A two-phase planning algorithm is ultimately suggested in this paper, which benefits from the advantages of both techniques. This paper is based on two-dimensional (2D) ultrasound imaged target regions for proof-of-concept purposes.

2 Problem Statement

The objective for the development of the current cryosurgery planning tool is to maximize freezing damage internal to the target region, while minimizing freezing damage external to the target region, all for a given number of cryoprobes N selected by the cryosurgeon. The outer surface of the target region in this study is defined as the outer contour of the prostate but excluding the urethra, which runs through the prostate. Consistent with clinical practice, it is further assumed that cryodamage is directly related to the thermal history of the tissue. Although the concept of the so-called lethal temperature is widely accepted by clinicians as the threshold temperature below which maximum cryodamage is achieved, the monitored parameter during cryosurgery is the freezing front via ultrasound imaging, which is likely to be associated with the isotherm of $0\,^{\circ}\mathrm{C}$ (i.e., the onset of crystal formation). Since currently accepted values for the lethal temperature are in the range of $-50\,^{\circ}\mathrm{C}$ to $-40\,^{\circ}\mathrm{C}$ [1,16] and cryodamage is assumed to gradually progress between the onset of crystal formation and the lethal temperature threshold, the isotherm of $-22\,^{\circ}\mathrm{C}$ has been selected here for planning. The optimal match of the latter isotherm with the contour of the target region is the objective of this planning, splitting the undesired effects of excessive cryodamage external to the target region and causing insufficient cryodamage internal to the target region. Nevertheless, the isotherm value of $-22\,^{\circ}\mathrm{C}$ is selected in the current work for demonstration purposes only, whereas its actual value is left to the decision of the cryosurgeon; the planning algorithms presented in the current work are independent of the value of the latter isotherm. The objective of planning can be formulated as follows:

$$G = \int_A w dA; \tag{1}$$

$$w = \begin{cases} 1 & -22\ ^\circ\mathrm{C} < T \quad \text{interior to the target area} \\ 0 & T \leq -22\ ^\circ\mathrm{C} \quad \text{interior to the target area} \\ 1 & T \leq -22\ ^\circ\mathrm{C} \quad \text{exterior to the target area} \\ 0 & -22\ ^\circ\mathrm{C} < T \quad \text{exterior to the target area} \end{cases}$$

where G is the target function, A is the cross-sectional area of the domain under consideration (including both the internal and external regions), and w is a spatial defect function determined by the local temperature distribution. The algorithm developed in this study is based on the underlying assumption that a simultaneous displacement of the N cryoprobes is considered to be an improvement over an initial placement, if the value of the objective function, G, decreases.

For the purpose of planning, the thermal history that would result from a specific layout of the N cryoprobes is predicted using heat transfer simulations. The selected heat transfer model for cryosurgery is the classical bioheat equation [17]

$$C\frac{\partial T}{\partial t} = \nabla(k \nabla T) + \dot{w}_b C_b (T_b - T) \tag{2}$$

where C is the volumetric specific heat of the tissue, T is the temperature, t is the time, k is the thermal conductivity of the tissue, $\dot{w}_b$ is the blood perfusion rate (measured in volumetric blood flow rate per unit volume of tissue), C_b is the volumetric specific heat of the blood, and T_b is the blood temperature entering the thermally treated area (typically the normal body temperature). The numerical scheme used to solve this model has been presented by Rabin and Shitzer [18]. Rabin and Shitzer have also shown that metabolic heat generation can be neglected during cryosurgery, and therefore it is omitted from Eq. (2). Although debates exist regarding the validity of this bioheat transfer model [19,20], experimental observations support its use for practical cryosurgery cases [21].

In this paper, a new two-phase optimization scheme is proposed for solving the cryoprobe layout problem. The first phase uses a modified version of the packing method [13–15] to find a geometrically uniform distribution of cryoprobes within the target region. This yields an effective initial guess of the optimal cryoprobe layout with a small computational cost. Starting from this initial layout, the second phase uses the force-field method [10], which has already been established, to further optimize the cryoprobe layout based on the evaluation of the temperature distribution calculated by bioheat transfer simulation.

3 Phase I of Optimization: Bubble-Packing

When the thermophysical properties and blood perfusion rate are virtually uniform throughout the simulated region, the shape of the target tissues becomes the most important factor in planning the optimum layout of the cryoprobes. It is thus reasonable to assume that an evenly spaced layout of cryoprobes would be close to the optimal plan. The definition of optimum layout is associated with the resulting temperature distribution around the cryoprobes and it is addressed in Sec. 4 of this paper. This section focuses on a technique to evenly distribute the cryoprobes, which adopts a previously developed computational method, called "the bubble-packing method" [13–15]. Whereas the original bubble-packing method was developed to find well-spaced locations of finite element mesh nodes, in the current research it has been modified and extended to address the cryoprobe layout problem.

Bubble-packing is a physically based approach that efficiently finds an even distribution of an arbitrary number of points inside a given geometric domain. The method first generates spherical elements called "bubbles" inside the domain. It then defines van der Waals-like forces between bubbles. With this proximity-based interbubble force, two adjacent bubbles attract each other when they are too far apart and repel each other when too close. Physically based relaxation is then applied to find a tightly packed, force-balanced configuration of bubbles, which usually is a repeating hexagonal arrangement—a pattern often observed in nature.

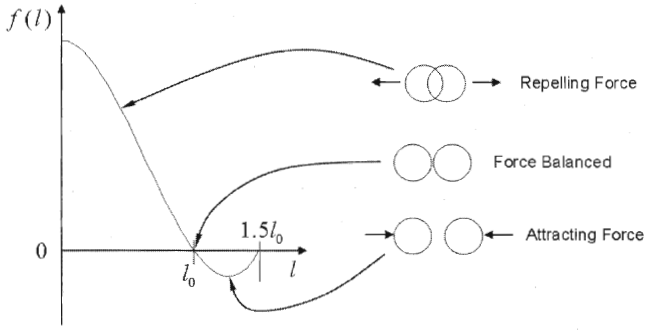

Fig. 1 The interbubble forces between adjacent bubbles are defined by a piecewise third-order polynomial function, Eq. (3)

In Phase I, the layout of cryoprobes is obtained by first packing bubbles tightly in the target region and then placing cryoprobes at the center of each bubble. Whereas the original bubble-packing method adaptively adjusts the number of bubbles for a tightly packed configuration, the modified version developed in this study adaptively adjusts the volume of the bubbles, since the number of bubbles—or cryoprobes—is specified by the cryosurgeon. The rest of this section presents the details of the implementation of bubble-packing and adaptive volume control.

3.1 Interbubble Force. The interbubble force between two adjacent bubbles is defined by mimicking the van der Waals force, using a piecewise cubic polynomial function (Fig. 1)

$$f(l) = \begin{cases} al^3 + bl^2 + cl + d & 0 \leq l \leq 1.5l_0 \\ 0 & 1.5l_0 < l \end{cases} \tag{3}$$

and

$$f(l_0) = f(1.5l_0) = 0, \quad f'(0) = 0, \quad f'(l_0) = -k_0 \tag{4}$$

where l is the distance between two bubbles, l_0 is the stable distance, and k_0 is the corresponding linear spring constant at l_0. When two adjacent bubbles are located closer than the distance l_0, a repelling force is exerted on both bubbles; when they are farther than l_0 but closer than $1.5l_0$, an attractive force is exerted, and no force will be exerted when they are greater than $1.5l_0$. When the arrangement of the bubbles is not uniform, interbubble forces make the system unstable and move the bubbles to a more uniform configuration.

3.2 Physically Based Relaxation. In order to find a force-balanced (or uniform) distribution of bubbles, Shimada et al. [13] used a numerical simulation of bubble dynamics, combined with a physically based relaxation, instead of the conventional multi-dimensional root-finding method. The physically based relaxation is advantageous in Phase I because it rapidly and continually finds new solutions when the simulation parameters, such as the number of cryoprobes and shape of the target region, are changed. This is convenient when the system is used intraoperatively; the system can reconfigure the layout of the cryoprobes quickly when the surgeon changes the surgical plan during the planning phase of the operation.

Given the proximity-based interbubble forces defined above, the goal of physically based relaxation is to find a bubble configuration (or a cryoprobe layout) that yields a static force balance. Assuming a point of mass at the center of each bubble and the effect of viscous damping, the proposed relaxation method finds a force-balanced configuration of bubbles by solving the following equation of motion:

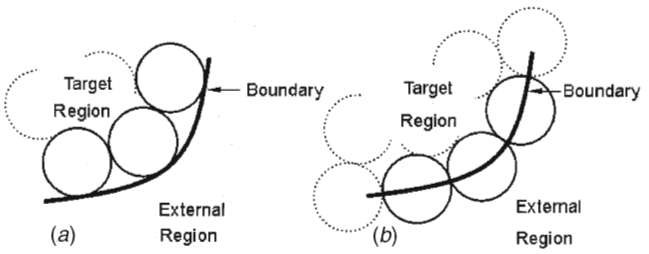

Fig. 2 Boundary conditions for bubble-packing: (*a*) in the current method, where bubbles are limited to the target region, and (*b*) in the original bubble-packing scheme [13], where bubble centers are placed on the contour of the target region; in cryosurgery, this would cause external cryoinjury

$$m_i \frac{d^2x_i(t)}{dt^2} + c_i \frac{dx_i(t)}{dt} = f_i(t), \quad i = 1, \ldots, n \tag{5}$$

where m_i, x_i, and c_i denote the mass, position, and damping coefficient of the ith bubble, respectively. Note that $f_i(t)$ is the sum of interbubble forces exerted on bubble i by all its adjacent bubbles. This second-order ordinary differential equation is numerically integrated by the standard numerical integration scheme of the fourth-order Runge-Kutta method [22].

In order for this second-order system to quickly reach a force-balanced configuration, it is critical to select an appropriate set of physical parameters for the mass, damper, and spring. If the interbubble force is too strong compared to the damping effect, the system becomes too responsive and suffers from excessive oscillation, yielding a slow convergence to a force-balanced configuration. However, if the interbubble force is too weak, the system becomes overdamped, delaying the convergence to a force equilibrium. To solve this problem, the following optimal damping coefficient has been suggested [13,23]:

$$\zeta = \frac{c}{2\sqrt{mk}} \cong 0.7 \tag{6}$$

3.3 Boundary Conditions. In this study, one of the modifications made to the original bubble-packing method [13] is a new type of boundary condition to prevent bubbles from moving out of the target region. The new method keeps the entire volume of each bubble inside the target region, as shown in Fig. 2(*a*), while the original method distributed bubbles on the boundary as well, as shown in Fig. 2(*b*). The new method is consistent with limiting the freezing injury to the target region.

3.4 Adaptive Volume Control. It is crucial to find the appropriate bubble size to space them evenly in a target region. As illustrated in Fig. 3, if the bubble size is too large, bubbles are pushed away from the boundary, and they may overpopulate around the center of the target region. If the size is too small, a gap may develop between neighboring bubbles.

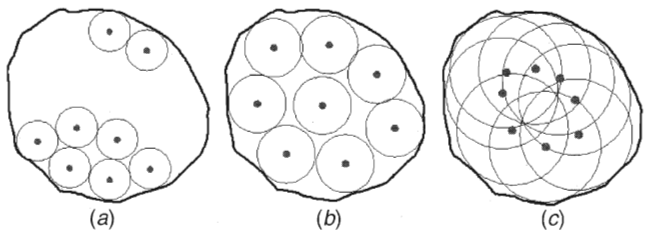

Fig. 3 The quality of bubble-packing is measured by the extent of overlapping: (*a*) bubbles with too little volume, (*b*) nearly appropriately sized bubbles by adaptive volume control, and (*c*) oversized bubbles

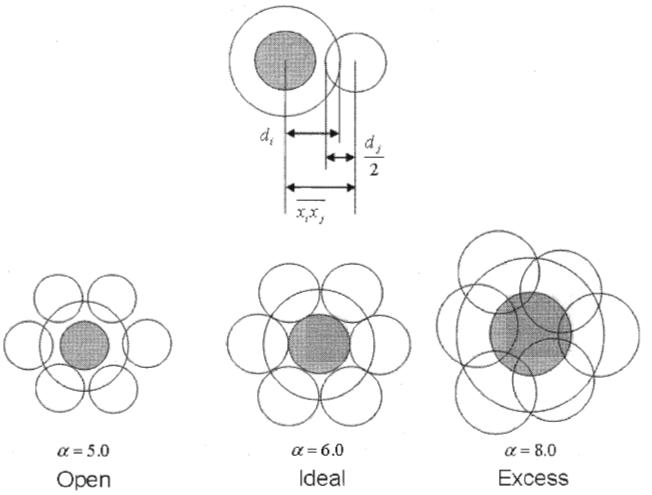

Fig. 4 Overlap of bubbles. The ideal overlap ratio in the two-dimensional case, α=6.0. Bubbles are located too sparsely when α<6.0, and too densely when α>6.0.

One possible criterion for the optimal bubble size is the amount of overlap between a bubble and its adjacent bubbles, as illustrated in Fig. 4, and formulated by Shimada [13]

$$\alpha_i = \frac{2}{d_i} \sum_{j=0}^{n} \left(d_i + \frac{d_j}{2} - \overline{x_i x_j} \right) \tag{7}$$

where α_i measures the overlap ratio for the ith bubble; d_i, d_j,x_i, and x_j are the diameters and locations of the ith and jth bubbles, respectively; and n is the number of adjacent bubbles to the ith bubble. The overlap ratio for an ideal, tightly packed configuration of bubbles in a two-dimensional problem is 6.0.

For the current application of cryosurgery planning, a major modification to the original bubble-packing method [13] is associated with the way the optimal bubble size is determined. In the modified scheme, the size of bubbles is adaptively adjusted to bring the overlap ratio as close as possible to the ideal value. This is quite different from the original method [13], which controls the population of bubbles in order to achieve high-quality triangular meshing in a given shape. Note that in the current study, the number of bubbles must remain constant because it corresponds to the number of cryoprobes to be used in the cryosurgery, as specified by the cryosurgeon.

Once the system reaches equilibrium of the forces for a given size of bubbles, the overlap ratio is calculated and the diameter of the bubbles is updated according to

$$r_{\text{updated}} = \frac{\alpha}{\alpha_{\text{ideal}}} r_{\text{current}} \tag{8}$$

The change in the diameter causes changes in the interbubble forces and breaks the force equilibrium. This leads to a consecutive physically based relaxation procedure. This sequence continues—along with the adaptive size control—until the size and configuration of the bubbles converge to an equilibrium state with an improved overlap ratio.

It is emphasized that the objective of the bubble-packing phase is to evenly distribute the cryoprobes in order to shorten the optimization process in the following phase of planning. However, it is noted that the bubble size and the size of the frozen volume associated with a specific cryoprobe are not directly related. Each bubble has a finite size, and the bubble population quickly reaches a steady state, whereas the frozen volume depends on the duration of the cryoprocedure, as well as the freezing power of the cryoprobes. Furthermore, there is no thermal barrier between cryo-

probes in the frozen region, as could be expected from the bubbles' illustration. If cryoprobes of different power are used, it is possible to adjust the size of the respective bubbles to resemble this difference.

4 Phase II of Optimization: Force-Field Analogy

Phase II further refines the cryoprobe layout in Phase I. While Phase I is purely based on geometrical considerations, Phase II is based on bioheat transfer simulations of cryosurgery. The optimization technique used in Phase II is known as "the force-field method," presented previously [10] and described here briefly for the completeness of this report.

For the purpose of the force-field method, defect areas are defined as either areas external to the target region with temperatures below some temperature threshold or areas internal to the target region with temperatures above the same temperature threshold (see also Eq. (2)). Given the suggested layout of cryoprobes at the end of Phase I, a bioheat transfer simulation is performed, and the total defect area (the sum of all the defect areas in the process, Eq. (1)) is monitored as the simulation progresses. At the initiation of freezing, the total defect area occupies the entire target region, and the total defect area size is maximized. As the freezing process progresses, the total internal defect area decreases, while at some point external defect areas start to develop. The minimum total defect area reaches its minimum when the total internal defect area becomes identical in size to the total external defect area. This is the point of termination of the bioheat transfer simulation.

At the end of the bioheat transfer simulation, the force-field method uses the defects in the temperature field to directly drive the improved cryoprobe locations. A force is defined to attract the cryoprobes to the internal defective region and push them away from the external defective region. The total force applied to a cryoprobe is given by

$$\vec{F}_{nT} = \sum_m \frac{C_1 C_2}{|\vec{r}_{mn}|^q} w_m A_m \Delta T_m \vec{u}_{mn} \tag{9}$$

where $\vec{F}_{nT}$ is the net force vector applied to cryoprobe n by all of the defective regions, C_1 is a constant to scale the force, w_m is the weight function that switches off the force from the nondefective regions (see also Eq. (1)), A_m is the cross-sectional area associated with grid point m, $\vec{r}_{mn}$ is a vector from grid point m to the cryoprobe n, $\vec{u}_{mn}$ is a normalized version of $\vec{r}_{mn}$, and ΔT_m is the difference between the temperature threshold for optimization and the temperature at grid point m, i.e., $\Delta T_m = (-22\,^\circ\mathrm{C}) - T_m$ in the current study. For the defective region outside the prostate, ΔT_m is positive, whereas for internal defects it is negative, indicating a repulsive force for external defects and an attractive force for internal defects. The force applied by each defect is inversely proportional to the square of the distance from the defect to the cryoprobe. Thus, the force decreases rapidly with distance so that defects near a cryoprobe apply greater force than defects farther away. The rationale is that the cryoprobes nearest a defect are likely to have the largest influence on that defect. The force applied by a defect is also proportional to temperature difference ΔT_m, which allows defective regions with more significant temperature differences to apply larger forces, the goal being to accelerate the optimization process. In order to prevent gathering too many cryoprobes at the same location, a short-acting repulsive force is applied between cryoprobes

$$\vec{F}_{nP} = \sum_j \frac{C_3}{|\vec{r}_{jn}|^3} \vec{u}_{jn} \tag{10}$$

where $\vec{F}_{nP}$ is the net force vector applied to cryoprobe n by all of the other cryoprobes, j is the cryoprobe index, C_3 is a constant, $\vec{r}_{jn}$ is a vector from cryoprobe j to cryoprobe n, and $\vec{u}_{jn}$ is a normalized version of $\vec{r}_{jn}$. This force is inversely proportional to the cube of the distance between cryoprobes so that the force is negligible unless the cryoprobes are very near one another.

Table 1 Representative thermophysical properties of biological tissues used in the current study (T in degrees Kelvin) [25–27]

Thermophysical property	Value	
Thermal conductivity, k, W/m K	0.5	$T>273$
	$15.98-0.0567\times T$	$251<T<273$
	$1005\times T^{-1.15}$	$T<251$
Volumetric specific heat, C, kJ/m^3 K	3600	$T>273$
	15,440	$251<T<273$
	$3.98\times T$	$T<251$
Latent heat, L, MJ/m^3	300	
Blood perfusion heating effect, $w_b C_b$, kW/m^3 K	40	

At the end of the bioheat transfer simulation, the forces on the cryoprobes are computed and one or more cryoprobes are moved accordingly; this provides the configuration for the next iteration. Ordinarily, the process in Phase II repeats in this fashion for a number of iterations. Eventually, the next iteration will result in an increase, rather than a decrease, in the total defective region. This typically occurs when the configuration is nearly optimal and the particular cryoprobe moved was already at a (locally) optimal location. Because this occurs when the solution is nearly optimal, the iteration typically involves moving just one cryoprobe. When this happens, the program begins a backtracking procedure. The iteration is rejected, and the cryoprobe with the second largest force in the previous iteration is moved. If this results in another increase in the defective region, the program backtracks again, this time moving the cryoprobe with the third largest force. Backtracking continues until either an improvement is achieved or the program backtracks through all of the cryoprobes. In the former case, the program continues on in the usual way. In the latter case, a local optimum has been found and the program terminates.

The bioheat transfer simulations applied in this study were carried out using a finite difference numerical scheme, which solves Eq. (2) explicitly [18]. Table 1 lists typical thermophysical properties used in the current study. Recently, Rabin [25] studied the propagation of uncertainties in the above values into the bioheat transfer simulations.

5 Results and Discussion

The effectiveness of the two-phase optimization technique was studied with two computational experiments: one with an idealized prostate geometry and the other with a realistic prostate geometry extracted from ultrasound images. The first experiment was performed as a benchmark, comparing the new two-phase technique with our previous one-phase technique [10], where the latter is incorporated into the two-phase technique as Phase II. The second experiment comes as a proof-of-concept to demonstrate that the proposed method can find an optimum in a reasonable time frame, even in a less regular target region.

5.1 Idealized Prostate Geometry: A Benchmark Experiment. With reference to Fig. 5, the benchmark problem [10] included a circular target region 46 mm dia, placed at the center of a 120 mm × 120 mm square domain. The urethral warmer was represented by circle 6 mm dia, located 6 mm off the center of the target region. The initial temperature was set to 37 °C, and the urethral warmer temperature was kept at 37 °C throughout the simulation. A zero-heat flux boundary condition was applied, and the temperature change at this boundary was monitored. From symmetry considerations, only the upper half of

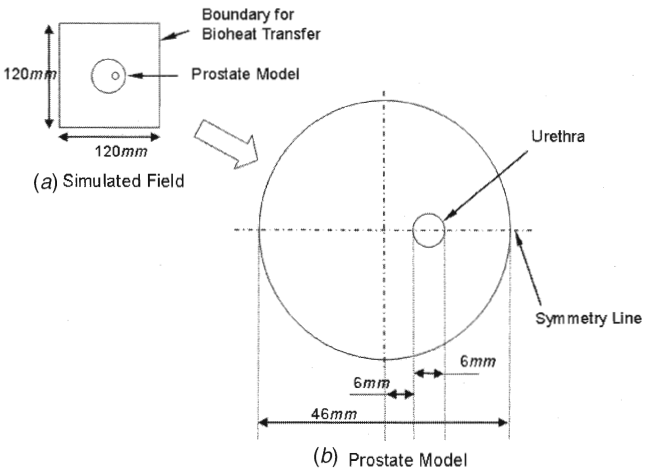

Fig. 5 Schematic illustration of the idealized prostate model used in the benchmark experiment: (*a*) the entire region simulated by means of a finite difference method and (*b*) the idealized prostate model

the region was simulated. For bioheat transfer simulations, the domain was represented by a 1 mm × 1 mm constant numerical grid. In terms of three significant digits, it was found that the outer boundary temperature did not deviate from its initial value throughout the simulation, which indicates that the domain behaves like an infinite domain in the thermal sense.

For the single-phase force-field analogy optimization, two methods of initial placement of the cryoprobes were benchmarked [10]:

(i) Distributing the cryoprobes in equal distances along a center circle (Fig. 6). The center of this circle lies on the straight line that connects the centers of the prostate and the urethra, where its radius is adjusted so that the circumference of the circle passes through the midpoints of the circumference of the prostate and the urethra.

(ii) Distributing the cryoprobes randomly in the target region.

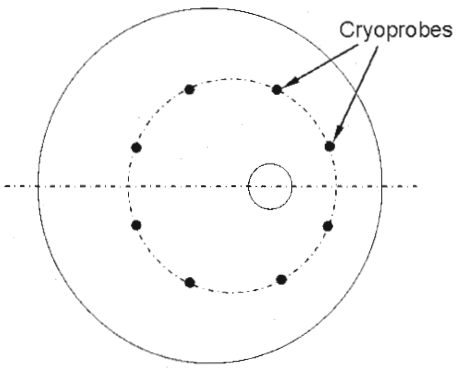

Fig. 6 Schematic illustration of the circular placement method of cryoprobes, prior to the force-field analogy phase

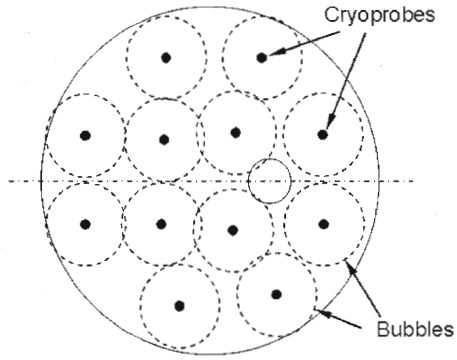

Fig. 7 Schematic illustration of the cryoprobe layout resulting from bubble-packing

Figure 7 illustrates the results for bubble-packing, which was used as an initial placement for Phase II in the two-phase protocol. A numerical simulation of bioheat transfer was performed immediately after bubble-packing, and the total defect area was taken as a measure of the quality of the bubble-packing phase. Immediately after, the force-field analogy phase followed.

Either in the single phase or in the two-phase optimization, planning was terminated once the defective region reached 5% of the target region size. The 5% threshold is chosen arbitrarily in this study, and obviously it is open for debate. Discussion about the possible implication of this value is given below.

Table 2 presents the total defect area after initial cryoprobes placement and before the force-field phase, whether using bubble-packing circular or random placement. It can be seen that the quality of bubble-packing increases with the increase in the number of cryoprobes, where circular and random placement techniques appear to be insensitive to the number of cryoprobes. It can be seen that by using bubble-packing alone, a total defect area of $<10\%$ is obtained for six or more cryoprobes. Furthermore, bubble-packing eliminates the need for Phase II altogether for the 14 cryoprobes and the 5% threshold arbitrarily selected in this study. In order to put these simulation results in context, one should compare the simulated results to the quality of imaging—most frequently ultrasound for prostate cryosurgery. Even if a full 3D ultrasound image could be obtained, it is likely that it would be associated with an uncertainty level of at least 5–10%. However, 3D ultrasound imaging of frozen regions is yet not available (the frozen image is opaque to ultrasound in the clinical frequency range), which requires the operation of simultaneous ultrasound transducers.

Table 2 Benchmark testing results for the problem illustrated in Fig. 5. Three different methods are tested for initial placement using bubble-packing, circular, and random, where the total defect area is compared before and after the force-field analogy phase (Phase II). Normalized values represent the time ratio of force-field analogy results to bubble-packing results.

Num. of probes	Total defect area at the beginning of forced-field method (%)			Number of force-field analogy iterations			Runtime of Phase II, min (normalized with respect to bubble-packing)		
	Bubble-packing	Circular placement	Random placement	Bubble-packing	Circular placement	Random placement	Bubble-packing	Circular placement	Random placement
14	3.9	22.0	31.0	0	22	26	4.9	66.9 (13.7)	51.2 (10.5)
12	6.2	21.5	35.5	6	20	59	12.8	70.9 (5.5)	141 (11.0)
10	7.0	20.8	41.2	6	14	37	13.8	49.5 (3.6)	100 (7.3)
8	6.8	17.7	31.5	10	8	38	30.2	34.2 (1.1)	270 (9.0)
6	9.2	19.3	60.5	12	6	23	55.2	37.9 (0.7)	173 (3.1)
4	16.6	24.4	23.3	19	17	16	228	240 (1.1)	234 (1.0)

Note that at least one bioheat transfer simulation is required to verify the quality of bubble-packing placement, and therefore even using 14 cryoprobes, the total runtime is about 5 min. Of this time, the actual bubble-packing procedure takes several seconds. Parallel efforts by our research group are now directed toward accelerating the bioheat transfer simulation runtime; the combination of such faster simulations with bubble-packing will likely lead to the practical application of computerized planning. Runtime benchmarks in this report are based on an AMD Athlon (TM) XP 3000+computer with a 2.10 GHz processor, a 400 MHz front side bus, and 1.00 GB of PC3200 DDR memory. The software was implemented with Visual C++. NET and executed under Windows XP Professional.

The total runtime, as well as the normalized runtime, are listed in Table 2, where normalization is done with respect to bubble-packing. It may appear that there is no advantage for using bubble-packing for six cryoprobes, when compared to force-field analogy combined with any of the other initial placement techniques. However, one should bear in mind that the threshold for termination of optimization plays a dramatic role in this comparison. For example, if a 10% total defect area threshold was selected as a termination criterion, the bubble-packing method would require about 5 min of runtime (similar to the 14 cryoprobes in Table 1), whereas the other two placement techniques will require somewhat less runtime, but similar in magnitude to the force-field procedure. This indicates that bubble-packing is dramatically faster for a greater number of cryoprobes. Although the random placement appears to be far less efficient, it is the only available alternative to bubble-packing in irregular-shaped target regions. This observation further demonstrates the superiority of the bubble-packing placement.

Figure 8 presents the temperature volume histograms (TVH) [24] for the optimal cryoprobe layout based solely on bubble-packing (Phase I). The reference value for external defect calculations is also the target area. It can be seen from Fig. 8 that over 90% of the target region is at temperatures of −45°C or lower, and that over 90% of the external region is at temperatures of 0°C or higher, for all the cases with more than four cryoprobes. The threshold value of −45°C is typically taken as the so-called lethal temperature. In this context, note that the isotherm for optimization is −22°C and not either of the above values.

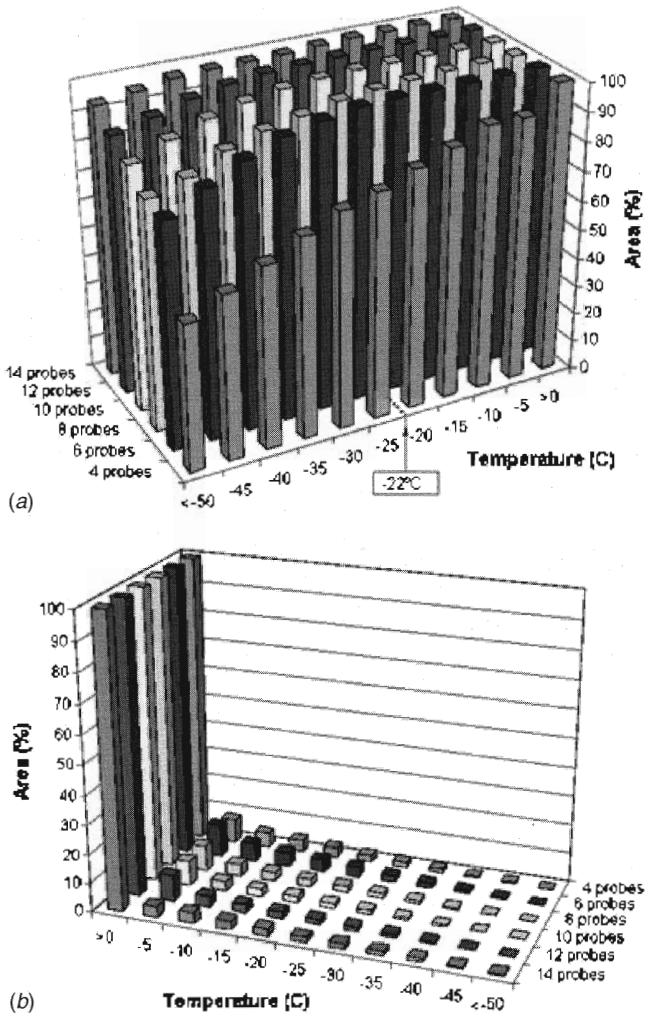

Fig. 8 Temperature volume histograms (TVH) of the prostate (*a*), and the external region (*b*), at the end of Phase I. Each bar represents the relative area which has temperatures of no less than the listed temperature.

5.2 Realistic Prostate Geometry: Proof-of-Concept. Figure 9 presents an axial ultrasound image of the prostate. This imaged prostate has an abnormal shape; the bottom is deformed upward, probably due to pressure induced by the rectal ultrasound transducer. The dark strip running from the center of the image upward is the shadow of the urethral warmer. The contour of the prostate and the urethral warmer were created manually, presented as dashed black and white lines. The longer dimension of the target region in this image is 42.5 mm, and the shorter dimension is 28.6 mm. A surrounding area of 105 mm × 105 mm was selected for heat transfer simulations in this experiment, with the contoured prostate placed at its center. Other conditions were kept similar to the previous computerized experiment. The experiment was repeated for 8, 10, 12, and 14 cryoprobes. Results of this experiment are listed in Table 3, selected temperature fields are shown in Fig. 10, and TVH are shown in Fig. 11.

Consistent with the previous experiment, 14 cryoprobes produced the smallest total defect area at the end of either phase. Phase II improved the planning of 14 cryoprobes from 6.8% to 5.4% at the expense of about 2.5 h runtime. This marginal improvement is shown in Fig. 10. Although results of Phase II show consistent improvement with increased cryoprobes, a similar trend is not necessarily observed for Phase I. Given the high cost of Phase II and its impractical duration, these results call for further optimization of the parameters of the bubble-packing algorithm.

In the operating room it is common practice to insert the cryoprobes through a placement grid, which is a metal plate having an x-y grid, typically in 5 mm increments. The placement grid limits the number of valid cryoprobe placements, an effect which is expected to shorten the runtime of Phase II. In the current work for example, a cryoprobe is allowed to be displaced in 1 mm increments on the numerical grid, which represents 25 valid cryoprobe locations for every valid point on such a placement grid. Taking this new constraint into account, Phase II could be expected to accelerate by an order of magnitude. Nevertheless, this research group plans to address the placement grid issue in future studies, after faster bioheat transfer simulations are developed.

5.3 3D Planning: Future Work. One of the most common practices in prostate cryosurgery today is the so-called pull-back method. In this method, the procedure is performed in two steps. All the cryoprobes are inserted into the same depth (in the z direction) in the first step, followed by a freezing/thawing process. All the cryoprobes are then pulled back at the same distance in the second step, before the consecutive freezing/thawing process is applied. While the clinician has a higher degree of freedom in placing cryoprobes on the x-y plane (typically, by using an x-y placement grid), the restriction of placing all the cryoprobes at the same depth in the first step and moving them back for the same interval in the second step dramatically lowers the possibility of minimizing the defect area (or of matching the frozen region with the target region). One could simplify and model each of the two

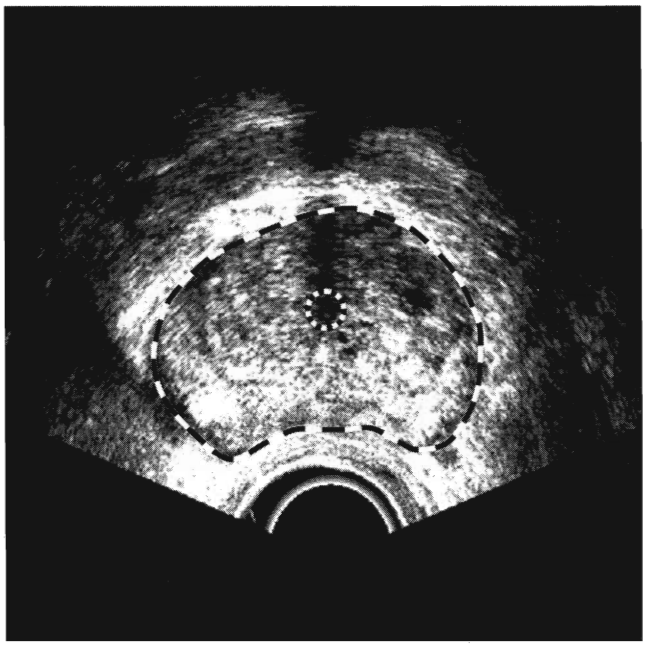

Fig. 9 Ultrasound image of the prostate area. The outer contour of the prostate and the inner contour of the urethra are highlighted with dashed lines.

steps of the pullback procedure as a 2D problem of planning. However, this simplification ignores some volumetric effects of the combined two-step procedure.

Although the mathematical formulation of both phases of optimization in the current study is rather general, and thus applicable to both 2D and 3D problems, the proof-of-concept presented in the current report is focused on simplified 2D cases. Developing a 3D planning algorithm is work-in-progress by the current research team. The axial movement in the z direction adds another degree of freedom for planning, and the defect area is expected to be significantly affected by this movement. Since cryoprobes cannot be moved to different locations on the x-y plane during the pullback, it is likely that different pullback distances in the z direction may reduce the defect volume and yield a better outcome for the cryoprocedure.

Another limiting factor in 3D planning is the cost of computation. The numerical scheme used in this study for heat transfer simulations works well in the 2D case, but is expected to be inadequate for the 3D case, where runtime increases dramatically. Developing a more time-efficient numerical scheme for bioheat simulations is the subject matter of parallel efforts by the current research team.

6 Summary and Conclusions

To date, cryoprobe localization is an art held by the cryosurgeon and based on the surgeon's own experience and accepted practices. Most frequently, cryoprobes are sequentially turned on and off toward the end of the freezing process in order to achieve a desired coverage of the target region. The need in this process is an evidence of suboptimal cryoprobe placement. Suboptimal cryoprobe localization may lead to one or more of the following deficiencies: areas in the target region may be left untreated, healthy surrounding tissue may experience cryoinjury, an unnecessary number of cryoprobes may be used, the duration of the surgical procedure may become excessive, and postcryosurgery complications may occur—all of which affect the quality and cost of medi-

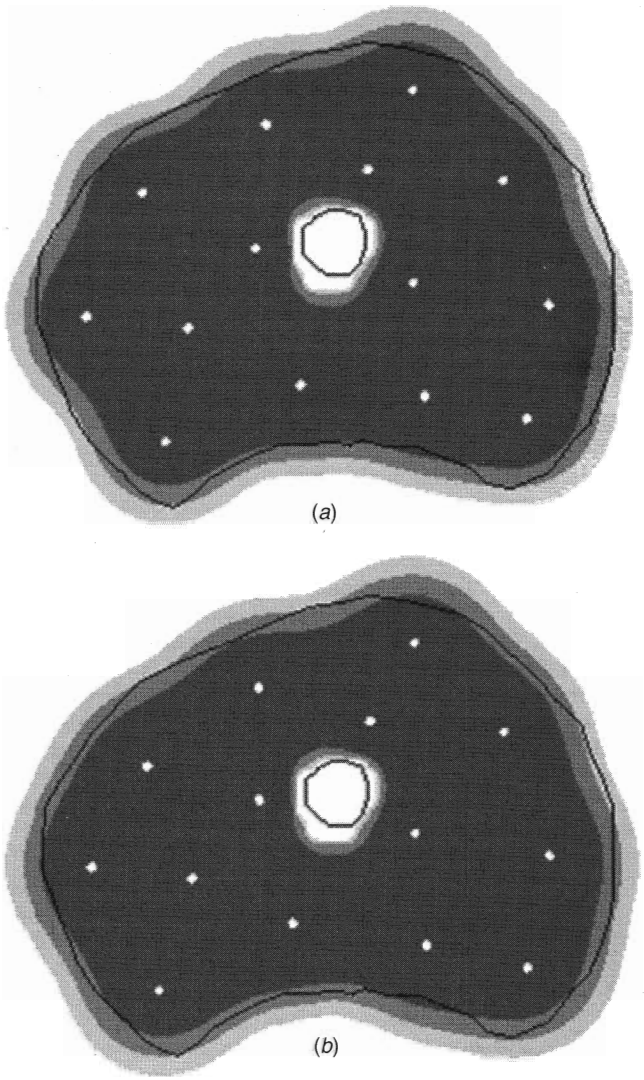

Fig. 10 Layout results for 14 cryoprobes at the end of Phase I (*a*) and II (*b*). The white, light, medium, and dark shades of gray correspond to areas with temperatures above 0°C, below 0°C, below −22°C, and below −45°C, respectively.

Table 3 Total defect area during two-phase planning on the prostate image shown in Fig. 9. Phase I is based on the bubble-packing method, and Phase II on force-field analogy.

	Phase I		Phase II		
Number of cryoprobes	Total defect region (%)	Runtime (sec)	Total defect region (%)	Runtime (min)	Num. of iterations
14	6.8	6	5.4	145	21
12	10.6	4	7.2	350	45
10	18.9	5	8.2	305	30
8	15.9	3	10.0	265	21

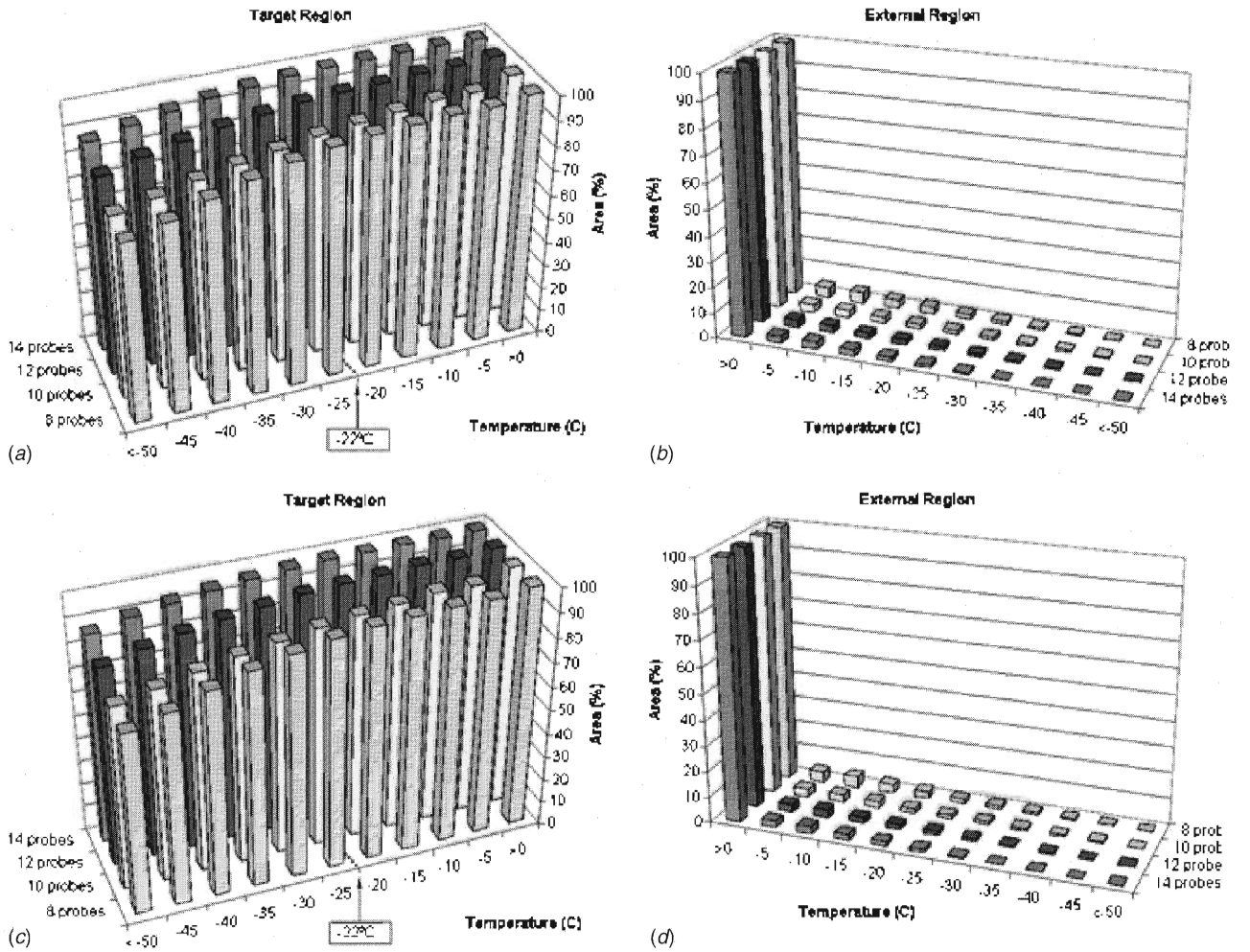

Fig. 11 Temperature volume histograms at the end of Phase I, internal (*a*) and external (*b*) to the target region, and at the end of Phase II, internal (*c*) and external (*d*) to the target region. Each bar represents the relative area which has temperatures of no less than the listed temperature. Simulated duration of cryosurgery at the end of Phase II is 4.6, 3.8, 2.8, and 2.5 min for 8, 10, 12, and 14 cryoprobes, respectively.

cal treatment. Computerized planning tools would help to alleviate these deficiencies, which is the subject of the current report.

A two-phase optimization method is proposed in this study, based on two previous and independent developments by this research team. Phase I is based on a bubble-packing method, previously used as an efficient method for finite elements meshing. Phase II is based on a force-field analogy method, which has proven to be robust at the expense of a typically long runtime. Nevertheless, the force-field analogy has shown to be orders of magnitude faster than any previous optimization techniques. The combination of bubble-packing in the first phase, with force-field analogy in the second, appears advantageous, where Phase I can be viewed as a shortcut by selecting an efficient initial layout for Phase II. It has been demonstrated that Phase I alone may be adequate in some configuration, whereas Phase II may be necessary in others. Either way, the objective function, associated with the minimum total defect area, will have to be evaluated at least once, based on bioheat transfer simulations, to verify adequate planning. More work is required in accelerating the bioheat transfer simulations in Phase II in order to make this phase practical for clinical applications; related research is currently underway by our research group indicating that runtime can indeed be made clinically adequate.

The major conceptual contribution in this study is that, in many instances, cryosurgery planning can be performed without the extremely expensive simulations of bioheat transfer; in some cases, the new scheme reduces planning runtime from hours to a few minutes. It is our belief that this runtime can be further shortened, and that the parameters of this technique can be optimized even more to efficiently cover a larger range of configurations and applications.

Acknowledgment

This project is supported by the National Institute of Biomedical Imaging and Bioengineering (NIBIB)—NIH, Grant No. R01-EB003563-01. The bubble-packing method is based, in part, on work supported under an NSF CAREER Award (Grant No. 9985288). We would like to thank Dr. Aaron Fenster from the Robarts Imaging Institute, London, Canada, for providing ultrasound images.

References

[1] Gage, A. A., and Baust, J., 1998, "Mechanisms of Tissue Injury in Cryosurgery," Cryobiology, **37**, pp. 171–186.

[2] Onik, G. M., Cohen, J. K., Reyes, G. D., Rubinsky, B., Chang, Z. H., and Baust, J., 1993, "Transrectal Ultrasound-Guided Percutaneous Radical Cryosurgical Ablation of the Prostate," Cancer, **72**(4), pp. 1291–1299.

[3] Chang, Z., Finkelstein, J. J., Ma, H., and Baust, J., 1994, "Development of a High-Performance Multiprobe Cryosurgical Device," Biomed. Instrum. Technol., **28**, pp. 383–390.

[4] Cohen, T. K., Miller, R. J., and Shumarz, B. A., 1995, "Urethral Warming Catheter for Use During Cryoablation of the Prostate," Urology, **45**, pp. 861–864.

[5] Keanini, R. G., and Rubinsky, B., 1992, "Optimization of Multiprobe Cryosurgery," ASME J. Heat Transfer, **114**, pp. 796–802.
[6] Kincaid, D., and Cheney, W., 1996, *Numerical Methods*, 2nd Ed., Brooks/Cole, Pacific Grove, CA.
[7] Vanderplaats, G. N., 1984, *Numerical Optimization Techniques for Engineering Design*, McGraw-Hill, INew York.
[8] Baissalov, R., Sandison, G. A., Donnelly, B. J., Saliken, J. C., McKinnon, J. G., Muldrew, K., and Rewcastle, J. C., 2000, "A Semi-Empirical Treatment Planning Model for Optimization of Multiprobe Cryosurgery," Phys. Med. Biol., **45**, pp. 1085–1098.
[9] Baissalov, R., Sandison, G. A., Reynolds, D., and Muldrew, K., 2001, "Simultaneous Optimization of Cryoprobe Placement and Thermal Protocol for Cryosurgery," J. Water Health, **46**, pp. 1799–1814.
[10] Lung, D. C., Stahovich, T. F., and Rabin, Y., 2004, "Computerized Planning for Multiprobe Cryosurgery using a Force-field Analogy," Comput. Methods Biomech. Biomed. Eng., **7**(2), pp. 101–110.
[11] Rabin, Y., Lung, D. C., and Stahovich, T. F., 2004, "Computerized Planning of Cryosurgery Using Cryoprobes and Cryoheaters," Technol. Cancer Res. Treat., **3**(3), pp. 227–243.
[12] Rabin, Y., and Stahovich, T. F., 2003, "Cryoheater as a Means of Cryosurgery Control," J. Water Health, **48**, pp. 619–632.
[13] Shimada, K., 1993, "Physically-Based Mesh Generation: Automated Triangulation of Surfaces and Volumes via Bubble-Packing," Ph.D. thesis, Massachusetts Institute of Technology, Cambridge.
[14] Shimada, K., and Gossard, D., 1998, "Automatic Triangular Mesh Generation of Trimmed Parametric Surfaces for Finite Element Analysis," Comput. Aided Geom. Des., **15**(3), pp. 199–222.
[15] Yamakawa, S., and Shimada, K., 2000, "High Quality Anisotropic Tetrahedral Mesh Generation via Packing Ellipsoidal Bubbles," 9th International Meshing Roundtable, pp. 263–273.
[16] Turk, T. M. T., Rees, M. A., Myers, C. E., Mills, S. E., and Gillenwater, J. Y., 1999, "Determination of Optimal Freezing Parameters of Human Prostate Cancer in a Nude Mouse Model," Prostate, **38**, pp. 137–143.
[17] Pennes, H. H., 1948, "Analysis of Tissue and Arterial Blood Temperatures in the Resting Human Forearm," J. Appl. Physiol., **1**, pp. 93–122.
[18] Rabin, Y., and Shitzer, A., 1998, "Numerical Solution of the Multidimensional Freezing Problem During Cryosurgery," ASME J. Heat Transfer, **120**, pp. 32–37.
[19] Charny, C. K., 1992, "Mathematical Models of Bioheat Transfer," *Advances in Heat Transfer*, J. P. Hartnett, T. F. Irvine, and Y. I. Cho, eds., Academic Press, New York, 19–156.
[20] Diller, K. R., 1992, "Modeling of Bioheat Transfer Processes at High and Low Temperatures," *Advances in Heat Transfer*, J. P. Hartnett, T. F. Irvine, and Y. I. Cho, eds., Academic Press, New York, pp. 157–358.
[21] Rabin, Y., Coleman, R., Mordohovich, D., Ber, R., and Shitzer, A., 1996, "A New Cryosurgical Device for Controlled Freezing, Part II: In Vivo Experiments on Rabbits' Hind Thighs," Cryobiology, **33**, pp. 93–105.
[22] Press, W. H., 1988, *Numerical Recipes in C: The Art of Scientific Computing*, Cambridge University Press, Cambridge, England.
[23] Ogata, K., 1970, *Modern Control Engineering*, Prentice-Hall, Englewood Cliffs, NJ.
[24] Drzymala, R. E., Mohan, R., Brewster, L., Chu, J., Goitein, M., Harms, W., and Urie, M., 1991, "Dose-Volume Histograms," Int. J. Radiat. Oncol., Biol., Phys., **21**, pp. 71–78.
[25] Rabin, Y., 2003, "A General Model for the Propagation of Uncertainty in Measurements into Heat Transfer Simulations and its Application to Cryobiology," Cryobiology, **46**(2), pp. 109–120.
[26] Altman, P. L., and Dittmer, D. S., 1971, *Respiration and Circulation* Federation of American Societies for Experimental Biology (Data Handbook), Bethesda, MD.
[27] Rabin, Y., and Stahovich, T. F., 2002, "The Thermal Effect of Urethral Warming During Cryosurgery," CryoLetters, **23**, pp. 361–374.